Supporting Information

One-step fabricating high energy storage polymer film with wide bandgap and high melting temperature induced by fluorine effect for high temperature capacitors applications with ultra-high efficiency

Jie Xiong, Guanxiang Zhang, Shaobo Tan, Honghong Gong, Yunchuan Xie*, Xiao Zhang, and Zhicheng Zhang**

Experimental section

Materials

The Parylene dimers, namely N-type and F-type dimer, were purchased from Su Zhou Pai Hua Layer Co., Ltd. All the other chemicals are commercially available and used as received until notified specially.

Preparation of Surface Functionalized Films

Typical CVD surface deposition includes the following three steps,

(1) Vaporizer The process starts with granular dimer. The Parylene dimer is vaporized from a solid directly into a Parylene dimeric gas. Temperature is 150-200°C.

(2) Pyrolysis The dimeric gas is heated to split the dimer molecule and produce a monomeric gas. Temperature is 600-700°C.

(3) Polymerisation The monomer gas is released into the coating chamber and deposited on the substrate surface to form a transparent polymer film. Deposition temperature is at room temperature, pressure is 30-50 mTorr, and deposition rate is 0.5-5 μm/h.

Instruments and characterization

Fourier transform infrared (FTIR) spectroscopy of the film was recorded on a Tensor 27 (Bruker, Germany) using the Attenuated Total Reflection (ATR) mode in the range of 4000 cm^{-1}–400 cm^{-1} to identify the chemical composition of samples. X–ray photoelectron spectroscopy (XPS) was recorded using X–ray photoelectron spectra (Thermo Fisher ESCALAB Xi^{+}) with an Al Kα source. Field–emission scanning

electron microscopy (FE–SEM) results were obtained on ZEISS GeminiSEM 500, and the samples were coated with a thin layer of gold before observation. Energy Dispersive X–ray Spectroscopy (EDS) mapping of a selected area in an SEM image was performed on the same instrument as SEM. Element mapping images and EDS spectra of mapped areas were recorded. For electric properties characterizations, gold electrodes with a thickness of 50–80 nm were sputtered on both surfaces of the polymer films with a JEOL JFC–1600 auto fine coater (Japan). The surface morphology of films was obtained by atomic force microscopy (AFM) (Dimension Icon, Bruker, Germany) in tapping mode. Broadband dielectric spectroscopy (BDS) was performed on a Novocontrol Concept 80 broadband dielectric spectrometer with temperature control. Storage modulus (E') and loss factor (tanδ) were obtained by dynamic mechanical analysis (DMA). For the investigations, a dynamic mechanical analyzer Netzsch DMA242E (Netzsch, Germany) was utilized. Measurements were performed in tensile mode at a constant frequency of 1 Hz. The temperature was varied between 30 and 180°C at a constant rate of 4°C min^{-1}. Prismatic samples of about 5 mm in width and 10 mm in length were used. The applied voltage was 1 V with the frequency changing from 10^0 Hz to 10^6 Hz and the temperature was increased from 20°C to 150°C at a rate of 4 °C min^{-1}; the electrode diameter of the test sample is 1 cm. The electric D–E hysteresis loops were collected on a Premiere II ferroelectric tester from Radiant Technologies, Inc. at room temperature, where AC electric fields ranging from 50 to 650 MV m^{-1} were applied across the polymer films with a triangular waveform at a frequency of 10 Hz. The breakdown electric field for polymer films was determined by the breakdown voltage tester (Beijing Beiguangjingyi Instrument Equipment Co. Ltd.) and the electric field applied rate of 1 kV min^{-1}. The diameter of the cylindrical electrode was 10 mm. The leakage current was obtained as less than 10 mA until the polymer films were broken down. Charge–discharge tests were performed using a PKCPR1502 test system (PolyK Technologies) with an applied electric field of 300 MV m^{-1} and resistance of load resistor of 100 kΩ. The charge–discharge cycle was controlled by a LabVIEW program.

The film samples were charged by isothermal surface potential decay (ISPD), and the needle tip was separated from the grid. The electrode is 5 mm, and the grid is 5 mm from the surface of the sample. The potentiometer was a Trek P0865 made in the United States, about 3 mm from the surface of the sample, and was placed in an incubator with the entire electrode system. The charging voltages applied to the needle electrode and the grid were –15 kV and –3 kV, respectively, charging for 10 min, then removing the voltage source, and moving the sample under the electrostatic probe for measurement. The test time was 2 h.

All quantum chemistry calculations were conducted by Gaussian 16 A.03 program. Unless otherwise specified, ωB97XD exchange-correlation functional in combination with 6−311+G(d,p) basis set. All wavefunction analyses were realized via the Multiwfn 3.7. All isosurface maps were drawn by VMD 1.9.324 based on the grid data generated by Multiwfn. The EEF was applied via “field” keyword in Gaussian program.

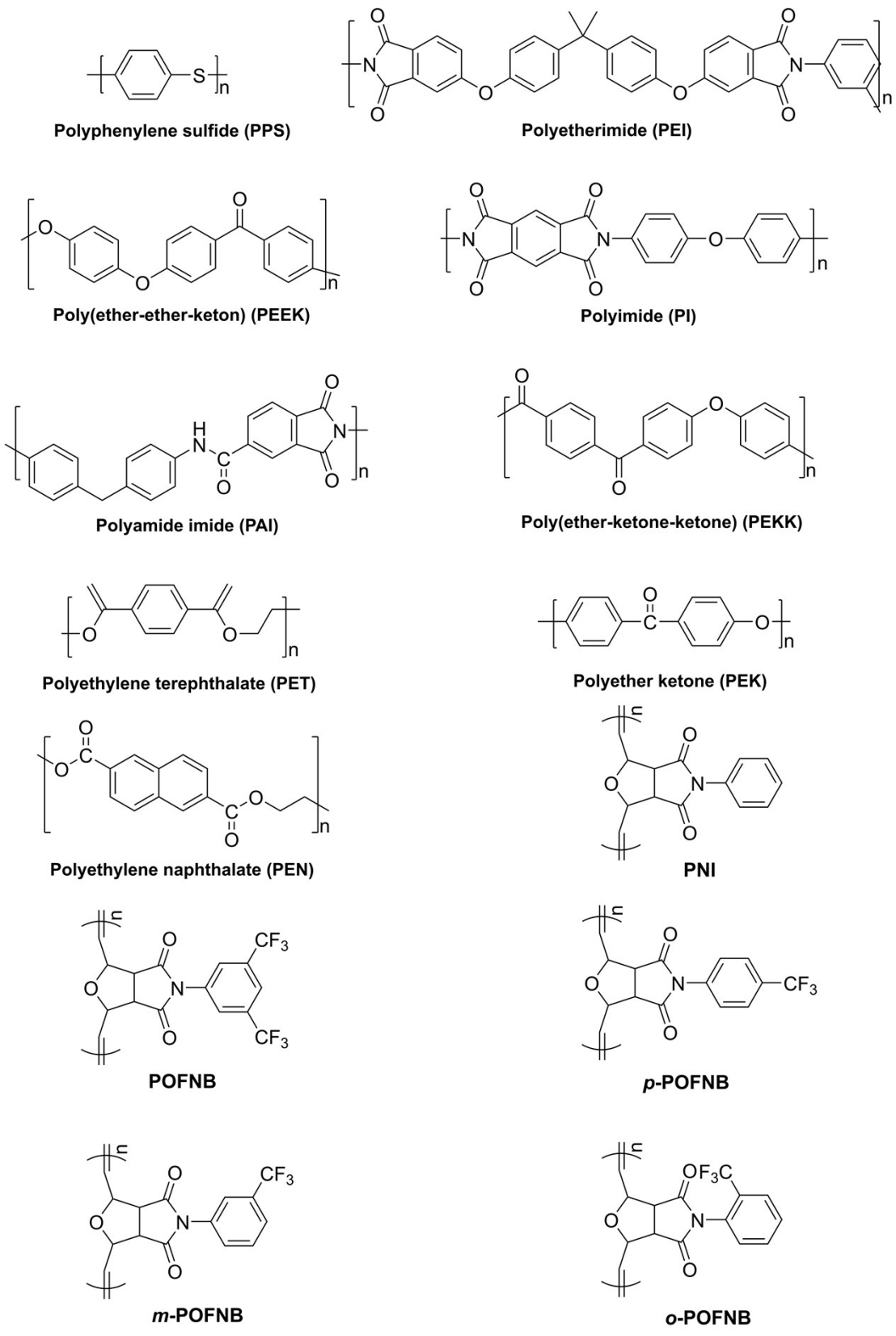

Figure S1. Chemical structures of high-temperature polymers.

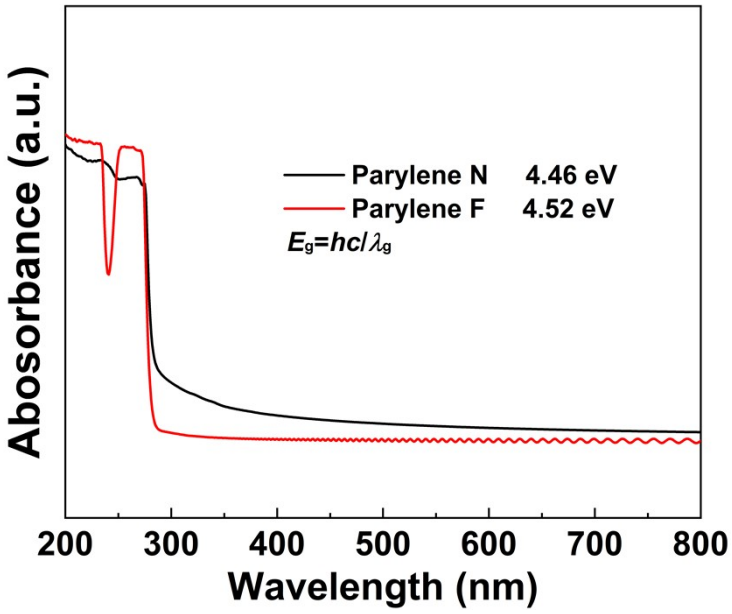

Figure S2. Optical bandgap of Parylene film derived from UV–vis spectroscopy.

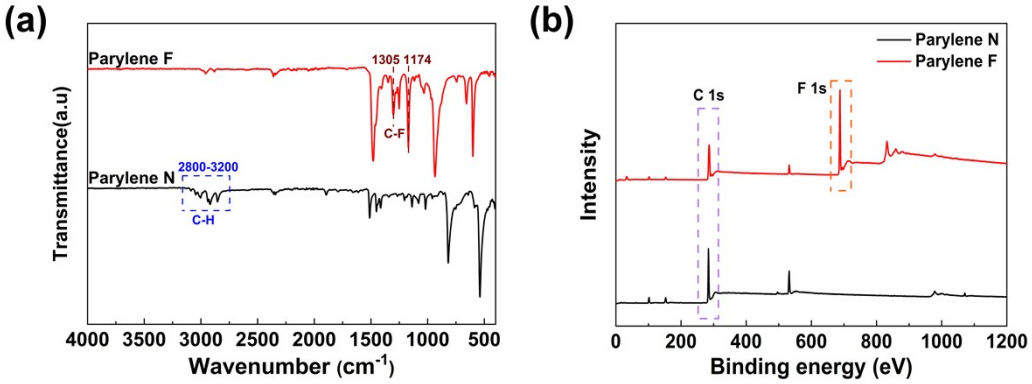

Figure S3. (a) FTIR and (b) XPS spectra of Parylene polymer films.

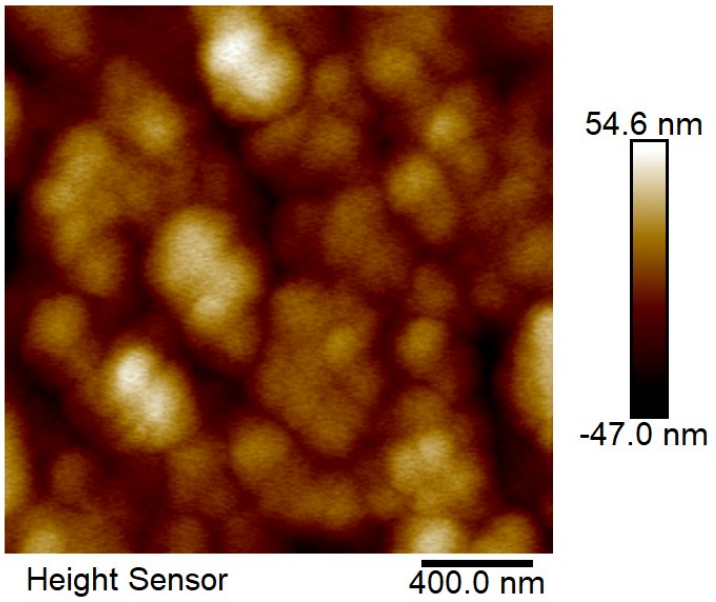

Figure S4. AFM topographic image of Parylene N film.

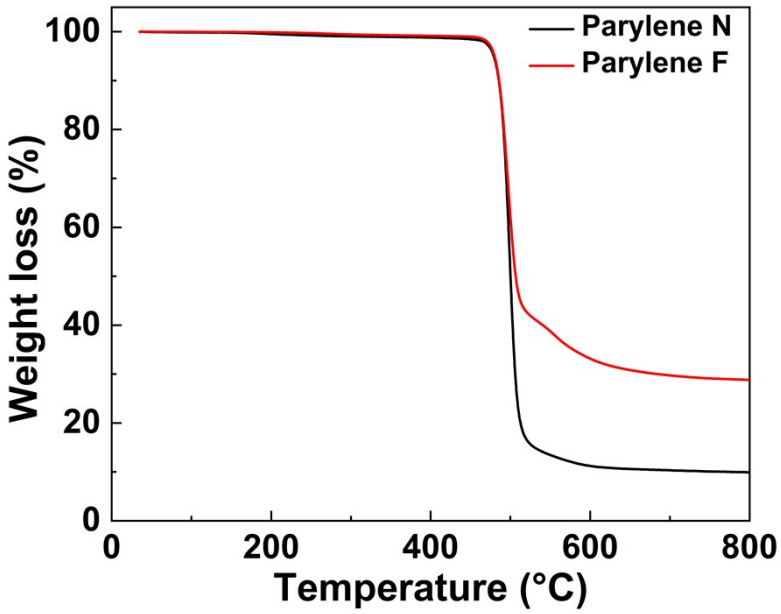

Figure S5. TGA curves of the Parylene films.

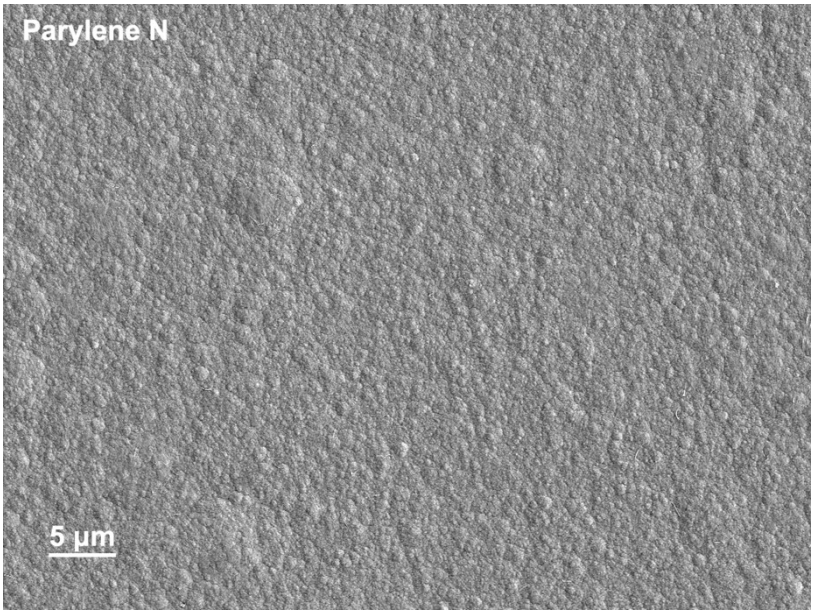

Figure S6. SEM images showing surface morphologies of Parylene N film.

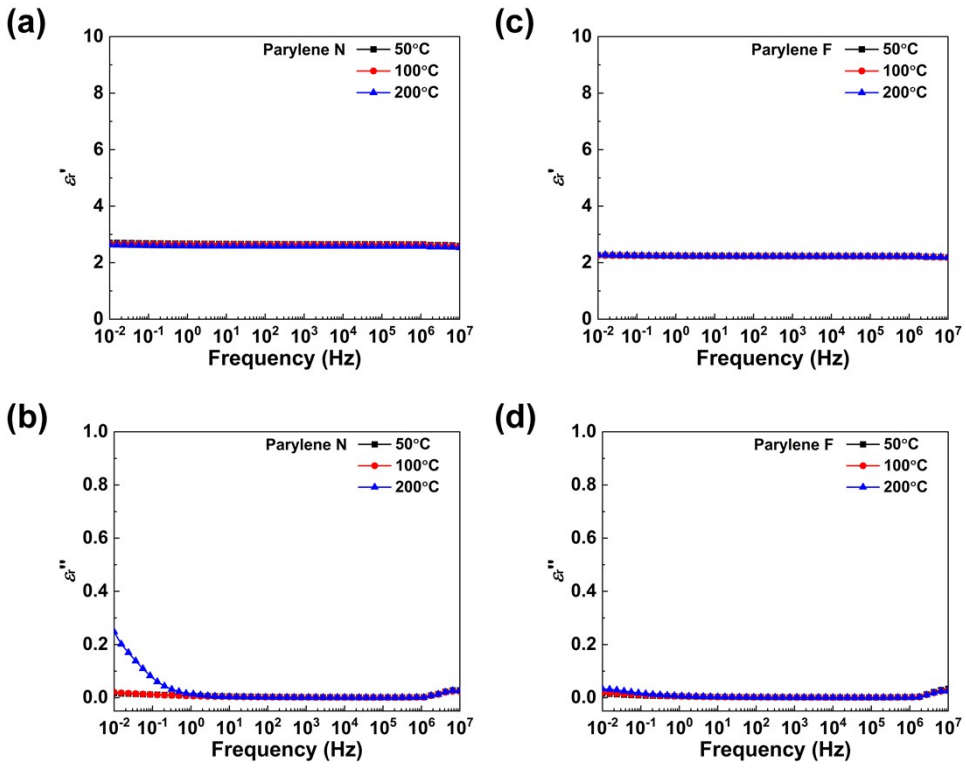

Figure S7. ε_r' and ε_r'' of (a,b) Parylene N, (c,d) Parylene F films as a function of frequency at difference temperatures.

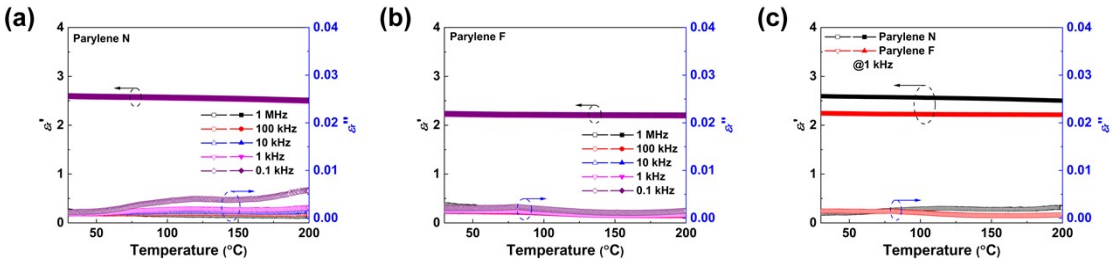

Figure S8. ε_r' and ε_r'' of (a) Parylene N, (b) Parylene F films as a function of temperature at different frequencies. (c) ε_r' and ε_r'' of parylene films as a function of temperature at 1 kHz.

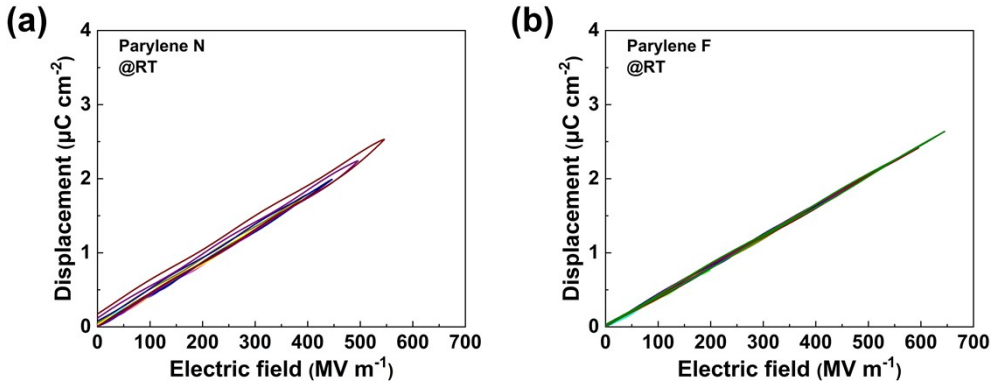

Figure S9. *D–E* loops of (a) Parylene N and (b) Parylene F films at room temperature.

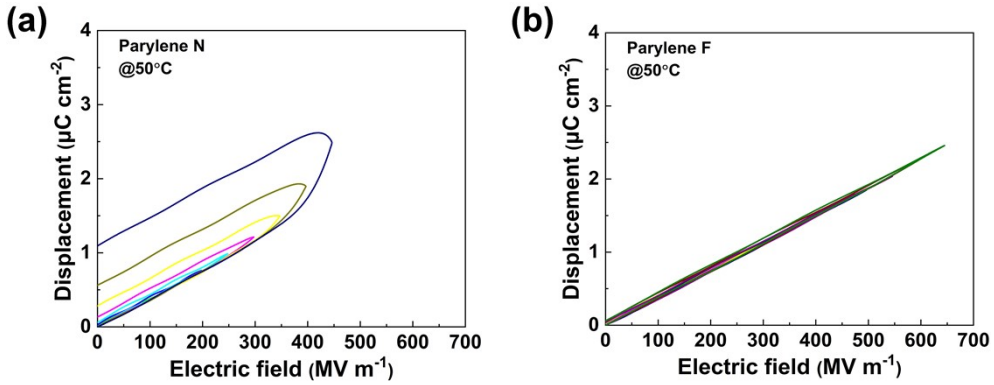

Figure S10. *D–E* loops of (a) Parylene N (b) Parylene F films at 50°C.

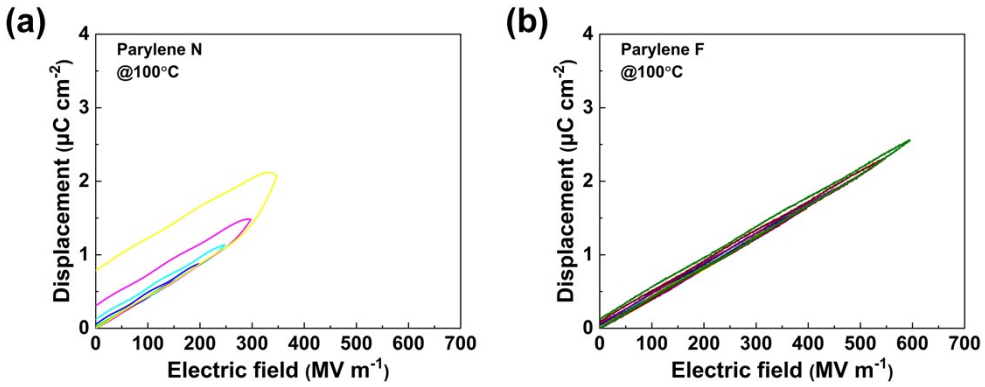

Figure S11. *D–E* loops of (a) Parylene N and (b) Parylene F films at 100°C.

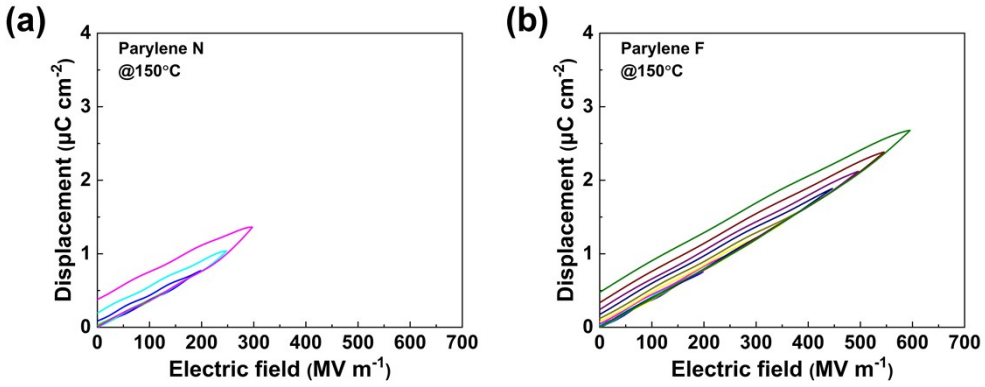

Figure S12. *D–E* loops of (a) Parylene N and (b) Parylene F films at 150°C.

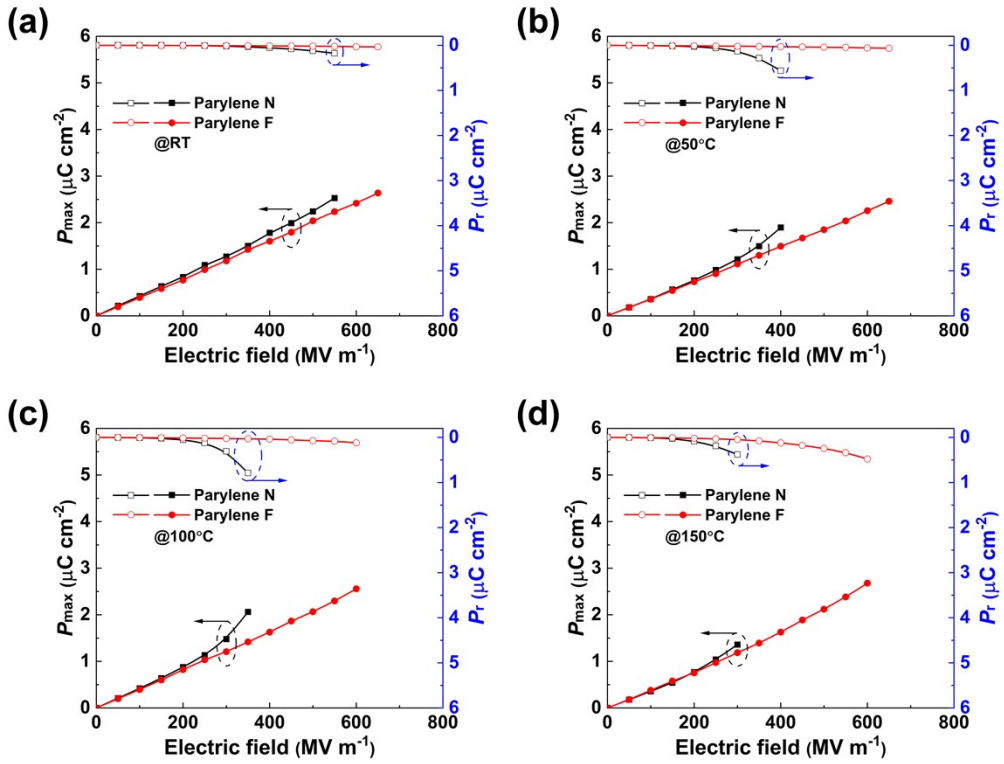

Figure S13. Displacement of Parylene films at (a) RT, (b) 50°C, (c) 100°C and (d) 150°C.

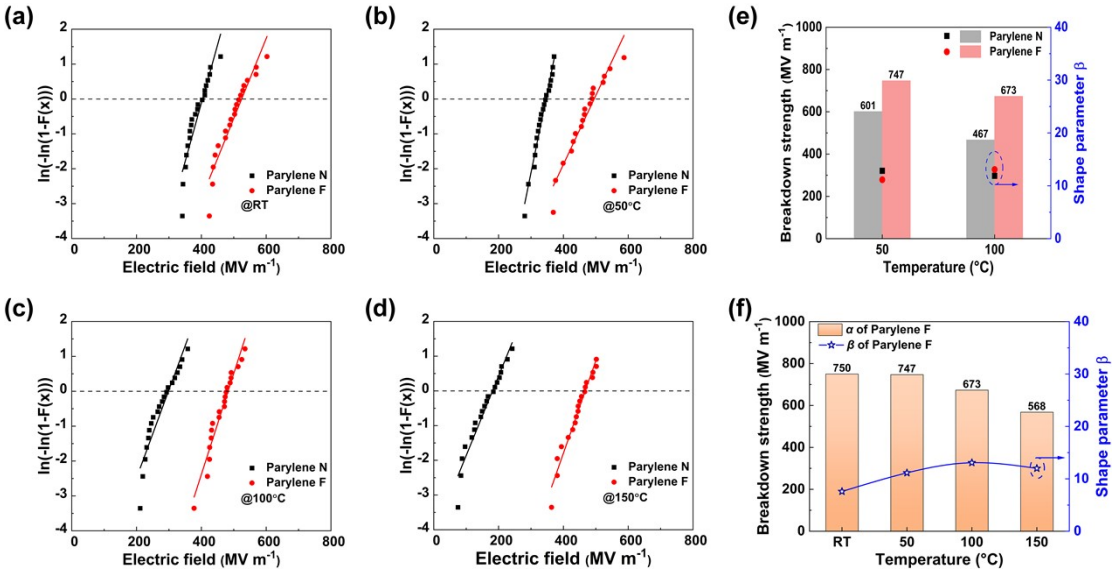

Figure S14. Weibull distribution of Parylene films at (a) RT, (b) 50°C, (c) 100°C and (d) 150°C. (e) E_b of Parylene films at 50 and 100°C. (f) E_b of Parylene F at different temperatures.

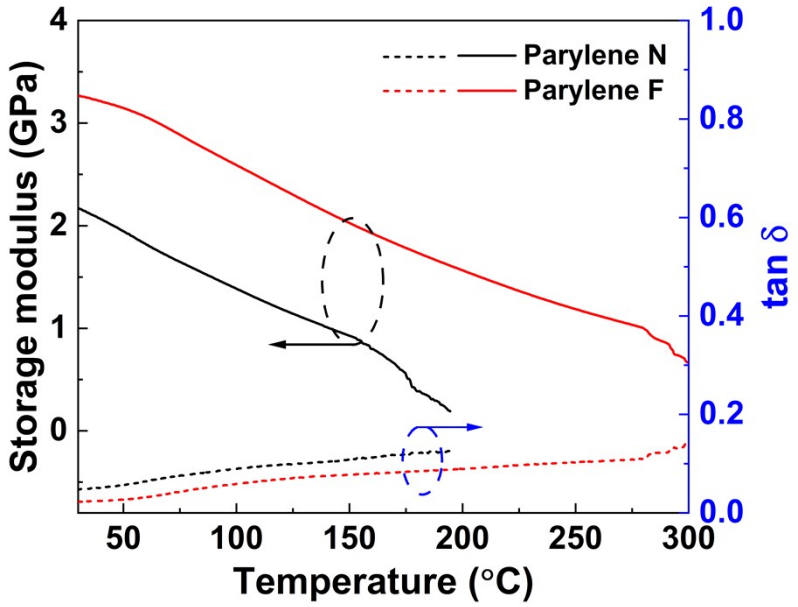

Figure S15. Storage modulus and tanδ of Parylene films.

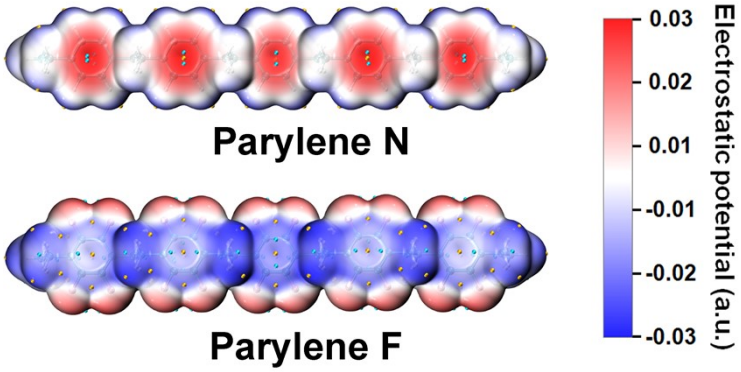

Figure S16. Simulated 3D electrostatic potential distribution of Parylene polymers. Blue and red colors represent negative and positive potentials, respectively.

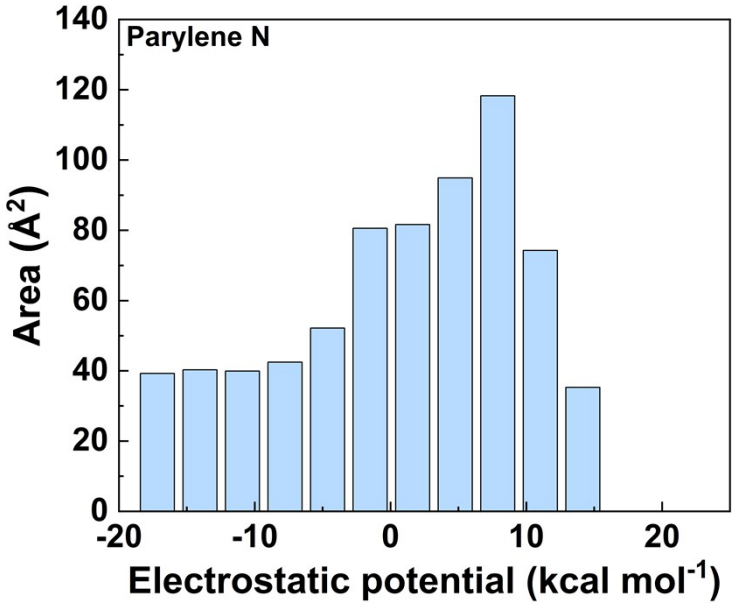

Figure S17. ESP area distributions of Parylene N.

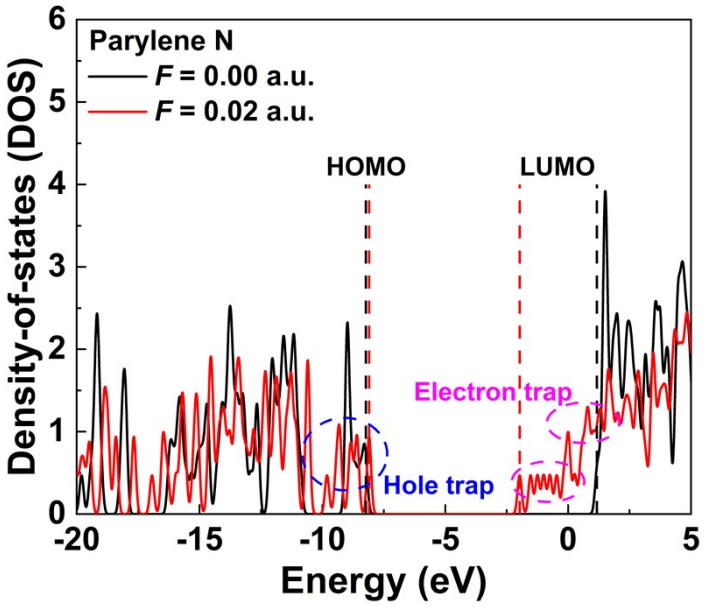

Figure S18. Density-of-state (DOS) curve of Parylene N.

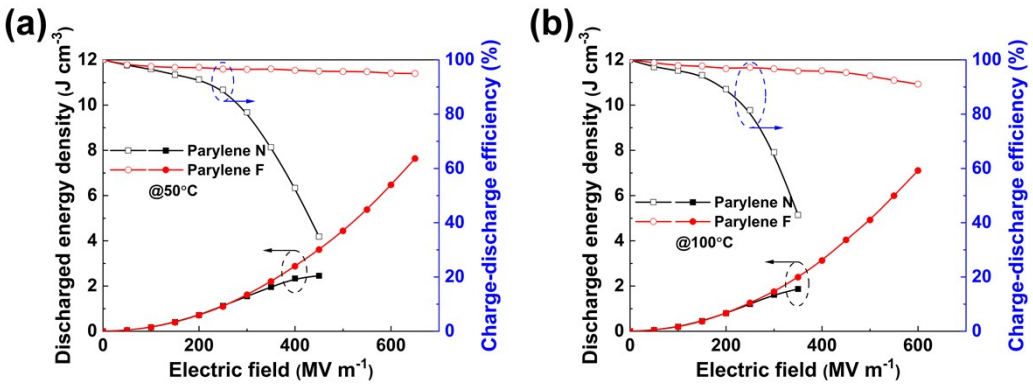

Figure S19. Discharged energy density and charge–discharge efficiency of Parylene films at (a) 50°C and (b) 100°C.

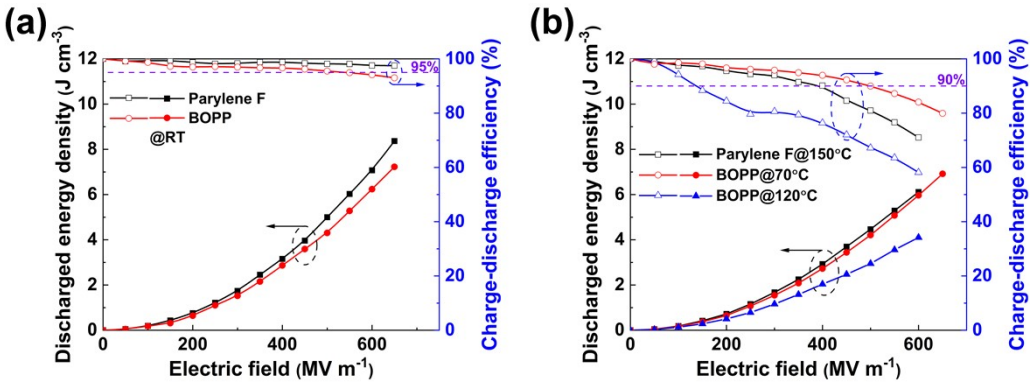

Figure S20. Discharged energy density and charge-discharge efficiency of BOPP and Parylene F derived from D-E loops at (a) room temperature and (b) elevated temperature.

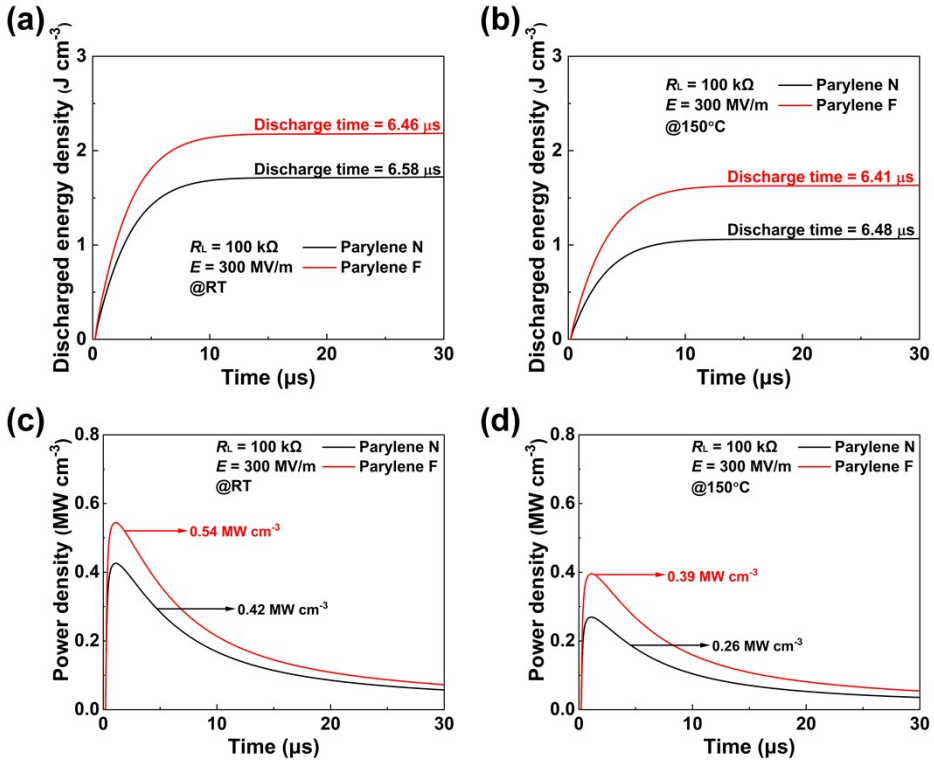

Figure S21. Discharged energy density as a function of time of Parylene films at (a) RT and (b) 150°C under 300 MV m^{-1}. Power density of Parylene films at (c) RT and (d) 150°C under 300 MV m^{-1}.